PAN
POLISH ACADEMY OF SCIENCES

Opto-Electronics Review

journal homepage: http://journals.pan.pl/opelre

Review of design and signal processing of polarimetric imaging cameras

G. Bieszczad*, S. Gogler, J. Świderski

Institute of Optoelectronics, Military University of Technology, 2 gen. S. Kaliskiego St., 00-908 Warsaw, Poland

Article info

Article history:
Received 23 Nov. 2020
Received in revised form 2 Jan. 2021
Accepted 7 Jan. 2021

Keywords:
thermovision, imaging polarimetry, optical system, optical architectures, image processing.

Abstract

Thermal-imaging systems respond to infrared radiation that is naturally emitted by objects. Various multispectral and hyperspectral devices are available for measuring radiation in discrete sub-bands and thus enable a detection of differences in a spectral emissivity or transmission. For example, such devices can be used to detect hazardous gases. However, their operation principle is based on the fact that radiation is considered a scalar property. Consequently, all the radiation vector properties, such as polarization, are neglected. Analysing radiation in terms of the polarization state and the spatial distribution of thereof across a scene can provide additional information regarding the imaged objects. Various methods can be used to extract polarimetric information from an observed scene. We briefly review architectures of polarimetric imagers used in different wavebands. First, the state-of-the-art polarimeters are presented, and, then, a classification of polarimetric-measurement devices is described in detail. Additionally, the data processing in Stokes polarimeters is given. Emphasis is laid on the methods for obtaining the Stokes parameters. Some predictions in terms of LWIR polarimeters are presented in the conclusion.

1. Introduction

Imaging polarimetry has been a subject of extensive research in leading scientific centres [1-4] in recent two decades. In astronomy, imaging polarimetry has been used since the 1970s. As the exploration of new exoplanets has become an important research field in the astronomical community in recent years, imaging polarimetry has emerged as a possible method for a direct imaging of exoplanets. For example, an imaging polarimeter, ExPol, is deployed at the William Herschel Telescope [5] and SPHERE at VLT [6]. In the microwave band, imaging polarimeters have been used by ESA and NASA during their missions aimed at examining ocean-water salinity or even modelling wind direction over sea surfaces [7-9]. For example, in ESA missions Soil Moisture Ocean Salinity (SMOS) a team from the Technical University of Denmark successfully designed and constructed a polarimetric radiometer, EMIRAD, which operated in the L band; the radiometer simultaneously registered two of Stokes parameters (S_0 and S_1) *via* two orthogonally polarized antennas. The remaining Stokes parameters (S_2 and S_3) were evaluated by computing, respectively, the real and imaginary parts of the cross-correlation function of the measured electric field. Other applications of imaging polarimetry include investigating the properties of soil plants vegetation [10], satellite-based research of Earth's atmosphere [11], examining state of water surfaces [12], medical diagnostics for cancer cell identification [13], biomedicine [14], and detecting military targets, as well as naval search and rescue missions [1,3,15].

When polarimetric imaging is used for a remote target detection (usually in the military applications, but not exclusively), four wavebands are usually considered: the visible (VIS), near infrared (NIR), mid-wave infrared (MWIR), and long-wave infrared (LWIR) wavebands. The polarized radiation in VIS and NIR spectra is dominated by reflected radiation, and, thus the measured signal primarily depends on an external source of radiation – the Sun [1]. It is characterized by a wide dynamic range and large spatial variations. Because the

*Corresponding author at: grzegorz.bieszczad@wat.edu.pl

https://doi.org/10.24425/opelre.2021.135824

measured polarimetric information significantly depends on the mutual geometry of the scene, source, and detector, the measured signal changes with a diurnal cycle, localization in the field and detector orientation. In the MWIR band, the measured radiation is attributed to both emission and reflection [3]. Generally, the polarized radiation in the MWIR accounts for only a small fraction of the radiation that reaches the detector. A fairly different situation occurs in the LWIR band, where the radiation is dominated by self-emission; additionally, because the scene is in thermal equilibrium (a temperature change usually occurs in a long time scale), polarization signatures can be relatively stable, and, thus they can be used as markers for detection [10,16]. However, polarimetric imaging in the LWIR band can be more challenging than in the case of shorter wavelengths, due to a lower detector resolution in the LWIR band and significantly higher costs of optical components [1].

Imaging polarimeters for LWIR and MWIR spectral windows, in which thermographic cameras operate, are built using cryogenically cooled, photonic focal-plane arrays (FPAs) or uncooled, microbolometrer detector arrays. Although cooled photon detectors perform three to five times better [17] than microbolometers in terms of noise equivalent degree of linear polarization (NEDoLP), they are significantly more expensive [18,19]. However, the development of the manufacturing technology of microbolometer detector arrays has enabled the fabrication of arrays with a high detector count (e.g., 640×480 and more). Commercially available LWIR polarimetric imager is depicted in Fig. 1 and two laboratory grade imagers are shown in Figs. 2 and 3.

Fig. 1. LWIR division of an FPA polarimetric imager developed by Polaris Sensor Technologies, Inc. (United States) [20].

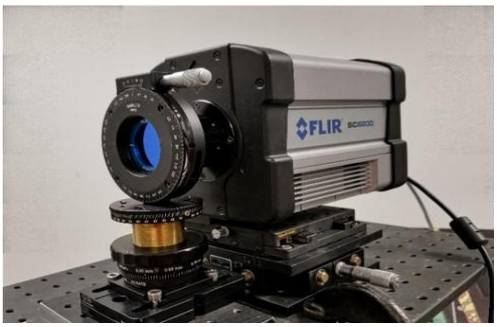

Fig. 2. Prototype of an LWIR division of a time polarimeter developed by FLIR Systems, Inc. (United States) [21].

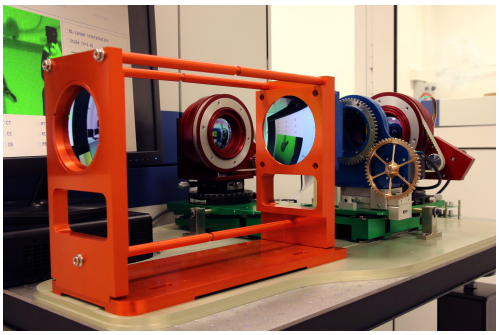

Fig. 3. Prototype of an LWIR divison of a time polarimeter developed at the Military University of Technology (Poland) [16].

Measuring the degree of linear polarization (DoLP) can help discriminate different features in a scene; these features would be otherwise indistinguishable from the background [1].

The polarisation state of incident radiation changes upon reflection off the object's surface. This change can help detect such an object, particularly the one made of dielectric materials. Furthermore, in the case of man-made objects, the plane of incidence is well defined, and, thus they are easily distinguishable from naturally occurring objects [1]. A relative magnitude of polarization components of the reflected radiation depends on angle of incidence, material properties (index of refraction), and surface properties of a reflecting object. The difference in reflection coefficients for different components of electric field and different refractive indices enables the detection of dielectric objects. This situation is depicted in Fig. 4.

Polarimetric devices can be divided into two categories, depending on the task performed: polarimeters for measuring light and those for measuring samples [23]. By using the Stokes polarimeter, an object can be characterized by determining the Stokes vector of the radiation reflected or emitted by the object [10,13]. Using the Mueller polarimeter, the object characteristics are determined using the Mueller matrices for transmittance and reflectance, i.e., by using information regarding how the polarization state of radiation passing through the object is modified [24]. The polarimeters designed for performing a remote object detection are always of the Stokes type.

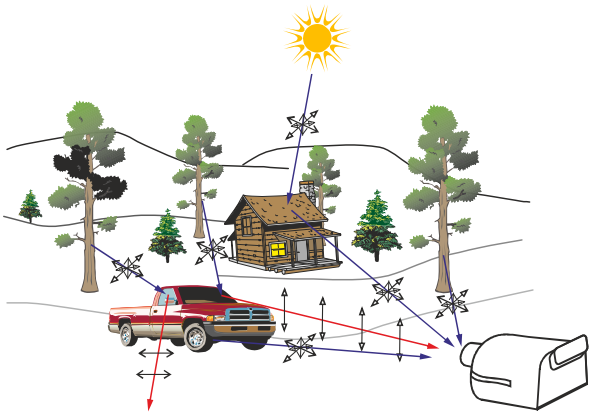

Fig. 4. Possible sources of a reflected linearly polarized light (red) and a non-polarized background radiation (dark blue) reaching a polarimteric sensor. Picture based on the one used in Ref. 22.

Polarization state in the Stokes formalism is usually represented as a column matrix of four elements, S_0, S_1, S_2, and S_3 which denote the total power of incident/initial radiation, power of radiation that is polarized horizontally or vertically, power of radiation that is linearly polarized with the azimuth of +45° or –45°, and power of radiation that is circular polarized (which represents the right- and left-handed circularly polarized radiant states), respectively. Notably, the first three parameters measurement is straightforward and requires only a linear polarizer. However, the measurement of the S_3 parameter requires a phase retarder. In the visible part of the spectrum, the measurement is usually not a problem, as wave plates are commonly used and are available off-the-shelf. However, in far infrared, phase plates are rarely used; additionally, uniaxial materials with a significant birefringence are few in number and usually are custom made, which makes them expensive. As W. Kudenov *et al*. [2] noticed however, the contribution of a circular polarization toward radiation that comes from a scene is usually insignificant; therefore, to obtain the necessary "polarimetric information," one need not quantify the S_3 parameter. Obviously, the lack of the quantification of S_3 makes the calculation of the degree of polarization which is defined as $\frac{\sqrt{S_1^2+S_2^2+S_3^2}}{S_0}$, impossible. However, it is still possible to determine DoLP, i.e., $\frac{\sqrt{S_1^2+S_2^2}}{S_0}$, and the azimuth of the ellipse, $\tan(2\psi) = \frac{S_2}{S_1}$. Therefore, knowing only parameters S_0, S_1, and S_2 enables one to discriminate objects on the basis of the DoLP and the azimuth of the ellipse of radiation reflected from their surfaces.

2. Polarimetric-measurement devices

Polarimeters designed for the Stokes-vector measurement can be classified according to the proposed taxonomy depicted in Fig. 5. Proposed taxonomy is a synthesis of similar ones described in Refs. 1 to 4.

To determine the Stokes parameters, it is necessary to take several measurements from which information about polarization can be extracted. There are various architectures of measurement systems enabling the Stokes parameters determinantion. These include the following:

- division of amplitude [2,4],
- division of time [14,17,21,25,26],
- division of aperture [3,5,6,27],
- division of image-plane [28-31],
- channeled spectropolarimeters [1,32,33].

Each has its own trade-offs regarding sensitivity, spatial and temporal resolution, system complexity in terms of size and weight, and developmental costs.

2.1 *Division of amplitude Stokes polarimeters*

In the case of division of amplitude polarimeters, beam-splitting elements are used to divide the incoming radiation into separate detection branches, each of which is dedicated to the measurement of a different Stokes parameter. The beam-splitting elements can be of polarizing or non-polarizing variety [4]. This solution was also used in the polarimetric camera, Spyder, manufactured by Polaris Sensor Technologies, Inc. [4]. Division of amplitude polarimeters are characterized by large dimensions and high implementation costs, as they require multiple detection matrices (minimum two). Additionally, the amount of energy that reaches each focal plane detector is smaller than that in other solutions due to power distribution on beam-splitting elements. However, their advantage lies in their ability to simultaneously determine three of the Stokes parameters (S_0, S_1, and S_2), i.e., real-time operation with a full FPA resolution. The polarimeter described in Ref. 4 can achieve a maximum DoLP rms error of 0.23% with an assumption of no S_3 component present.

2.2 *Division of time Stokes polarimeters*

A rotating polarizing element is used in division of time polarimeters. It is a device either with a polarizing element that sequentially rotates to a given set of azimuths or with a polarizing element that is continuously rotated. Polarimeter with sequential rotation is considered a snapshot polarimeter. The rotating polarizing element is a linear polarizer or a phase retarder. Advantage of this solution is the simplicity of both implementation and data processing to determine the Stokes parameters. However, a significant disadvantage is the limited registration speed. The image output frequency of an exemplary state-of-the-art polarimeter with a microbolometric detector array is in the order of several Hz [25]. This method assumes that the polarization state does not change during at least half rotation of the polarizing element; if this condition is not

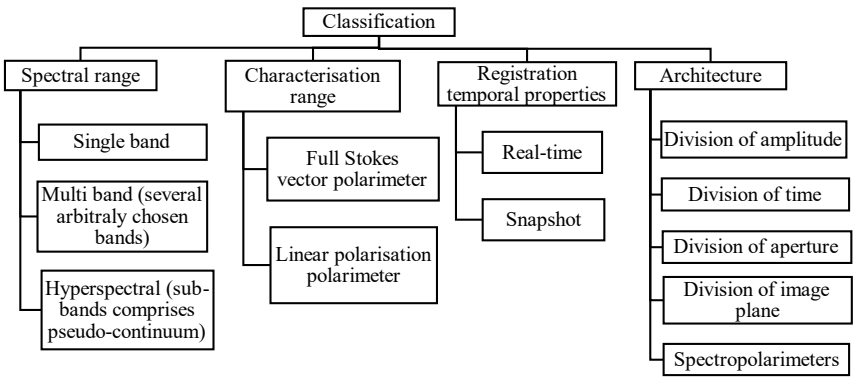

Fig. 5. Classification chart of the Stokes polarimeters.

met, a false polarizing signal appears in the image. Also, ideally, the rotated element should be perfectly plane-parallel. In the case wherein the polarizing element is continuously rotated, its rotation must be synchronized with the detector by using a phase-synchronization loop. This requires using the two-phase lock-in method [26]. The Stokes parameters can be determined using this method when a large number of samples are recorded for only one rotation period of the polarizing element.

2.3 Division of aperture Stokes polarimeters

In division of aperture polarimeters, miniature lenses are placed in the aperture stop plane (or in the plane of its image), each of which forms an image in the focal plane [27]. Often optical systems located in the pupil plane create images on one detector array, meaning that at the same time it is a method with division of the image plane. The optical design of such a system is complicated and its implementation costs are high compared to division of time or division of image plane systems. The formation of four images on one plane results in the loss of resolution and occurrence of a registration error, as each miniature lens forms the image of a slightly different region in the object space of the optical system. Division of aperture polarimeters are easier to align and the alignment is considered to have a better long-term stability compared to division of amplitude polarimeters. They require a field stop to sharply separate individual channels on the FPA. In the case of uncooled LWIR systems, the field stop would be a strong source of unwanted radiation.

2.4 Division of image plane Stokes polarimeters

Arrays of micro polarizers are used in division of image plane polarimeters. Each set of micropolarizers, placed in front of a single pixel of the matrix, forms a large so-called "super-pixel". This solution is conceptually analogous to the Bayer filter. The maximum number of micropolarizers is four: for horizontal, vertical, +45°, and –45° polarizations. This solution was described, among others, in Refs. 27 and 28. Notably, Thales introduced a matrix of polarization-sensitive QWIP detectors [30]. The matrix, made in a 1280×1024 resolution was sensitive to the radiation in the range of 8 - 12 μm. State-of-the-art microbolometer based solutions were presented in Ref. 30. For instance, a microbolometric Pyxis polarimetric imager, developed recently, can produce images with a 640×512 resolution and an NEDoLP of 0.5%, and with a framerate of 30 Hz (lens with F# = 0.85). However, a drawback of this type of solution is the loss of resolution, while the advantages are a compact design and a simultaneous registration of different polarization states. For microbolometric solutions very fast lenses are often a must due to a low sensitivity of such devices. Although with this technique one can only detect linear polarization states, it is sufficient for most applications. Polarimeters of this type, by definition, are subject to a registration error which is removed at the final signal processing stage; however, their optical design is significantly simpler compared with the previously discussed architectures.

2.5 Channeled spectropolarimeters

Registering the state of circular polarization (i.e., determining parameter S_3) requires a wave plate. If a device operates in a wide spectrum range, the retarder should be achromatic. In the case of the LWIR range, producing such elements requires special processes to synthesize crystals such as CdS and CdSe, which are specifically designed for this task, or the application of a diffractive sub-wavelength structure by using lithographic techniques (e.g., electron-beam lithography), both of which are expensive. One way to solve this problem is using a wavelength-selective detection. If individual wavelengths can be recorded separately, one can calibrate the chromatic retardance [1,32,33]. Advantage of this method is the possibility of obtaining additional information about the spectral information of each polarization state. This measurement method belongs to the category of snapshot methods and imaging is performed by scanning the object space (push-broom scanning). Despite a large potential, LWIR channelled spectropolarimeters have been rarely used in practical applications so far.

3. Data processing in Stokes polarimeters

Irrespective of how data in the imaging polarimeter is obtained, different ways exist to process the measured signal. Method of obtaining the Stokes parameters affects the overall architecture of the device to a certain extent. Three ways to determine the Stokes parameters used in modern devices are discussed in the following.

3.1 Data-reduction matrix

In the case wherein one measuring branch is a polarization-state analyser, the response P_m of the analyser on the incident radiation with a polarization state defined using the Stokes vector $\boldsymbol{S}$ equals [1,23]:

$$P_m = \boldsymbol{A_m} \cdot \boldsymbol{S} = a_{\mathrm{m}0}S_0 + a_{\mathrm{m}1}S_1 + a_{\mathrm{m}2}S_2 + a_{\mathrm{m}3}S_3, \quad (1)$$

where m is the consecutive measurement number.

To determine the Stokes vector of the incident radiation, Q measurements should be performed using Q analysers, $\boldsymbol{A}_m$, where $m = 0, 1, \ldots, Q-1$ is the consecutive measurement number. The measurement matrix $\boldsymbol{W}$ $(Q\ x\ 4)$ can be described as:

$$\boldsymbol{W} = \begin{bmatrix} \boldsymbol{A}_0^T \\ \boldsymbol{A}_1^T \\ \vdots \\ \boldsymbol{A}_{Q-1}^T \end{bmatrix}, \quad (2)$$

and the measurement vector $\boldsymbol{P}$ comprising Q responses becomes:

$$\boldsymbol{P} = \boldsymbol{W}\boldsymbol{S}. \quad (3)$$

The measured Stokes vector can be calculated as follows:

$$\widehat{\boldsymbol{S}_m} = \boldsymbol{W}^{-1}\boldsymbol{P} + \boldsymbol{\epsilon}, \tag{4}$$

where $\boldsymbol{W}^{-1}$ denotes the polarimetric data-reduction matrix and $\boldsymbol{\epsilon}$ is the error term.

In a special case of a complete type polarimeter where there is a separate measuring branch that corresponds to a measurement of each Stokes vector element, the analyser-sensitivity vector $\boldsymbol{A}$ is the smallest possible comprising Q = 4 orthogonal elements and is described as follows [1]:

$$\boldsymbol{A} = \begin{bmatrix} a_0 \\ a_1 \\ a_2 \\ a_3 \end{bmatrix} \propto \begin{bmatrix} I_H + I_V \\ I_H - I_V \\ I_{45} - I_{135} \\ I_{PS} - I_{LS} \end{bmatrix}, \tag{5}$$

where I_H and I_V denote the intensities of radiation components that are polarized horizontally and vertically, respectively; I_{45} and I_{135} denote the intensities of components that are polarized at 45° and 135° angle, respectively; I_{PS} and I_{LS} denote the intensities of components that are polarized circularly counter-clockwise and clockwise, respectively.

Considering Eq. (4), the following three cases exist:

- When $Q = 4$ and measurements are linearly independent, matrix $\boldsymbol{W}$ is a full rank and there exists an inverse thereof. Therefore, Eq. (4) has an unambiguous solution.
- When $Q > 4$, the system has more equations than the number of variables. In the presence of noise, all the equations are linearly independent; thus, the system is overdetermined, meaning that no unique solution exists for this system. In this case, a best-fit solution, in terms of the sum of least squares, can be found by estimating a generalized inverse (e.g., Moore–Penrose inverse) matrix or by applying QR factorization to matrix $\boldsymbol{W}$.
- When $Q < 4$, the rank of matrix $\boldsymbol{W}$ is three or less, and in this case, the polarimeter is incomplete, meaning that not all the parameters can be determined. A solution can be calculated by minimizing an objective function of choice, clearly indicating an optimization problem. A solution can also be estimated by posing some constraints on the solution space, the simplest and most common constraint being the assumption of a S_3 parameter to be zero.

3.2 Frequency analysis

Frequency analysis is especially appropriate for a polarization inspection because the value of polarized radiation periodically changes as a polarization state analyser is rotated with a constant angular velocity. This concept is extensively presented in Ref. 2. Response P_m represents a detector output to the incident radiation intensity value recorded for the subsequent azimuth positions of the polarizing element. If the polarizing element is rotated in discrete, constant-size steps, the signal spectrum is also discrete. In a frequently encountered scenario, where the polarization state analyser is a linear polarizer, the analyser vector is that of the first row of the Mueller matrix for a rotated polarizer, i.e. [1,24]:

$$\tfrac{\mu}{2}[1 \quad \cos(2\theta) \quad \sin(2\theta) \quad 0], \tag{6}$$

where μ is the polarizer efficiency. Given Q samples per one revolution, the measurement equation has the form of [1]:

$$\begin{bmatrix} P_0 \\ P_1 \\ \vdots \\ P_Q \end{bmatrix} = \tfrac{\mu}{2}\begin{bmatrix} 1 & \cos\left(2\frac{2\pi}{Q}\cdot 0\right) & \sin\left(2\frac{2\pi}{Q}\cdot 0\right) & 0 \\ 1 & \cos\left(2\frac{2\pi}{Q}\cdot 1\right) & \sin\left(2\frac{2\pi}{Q}\cdot 1\right) & 0 \\ \vdots & \vdots & \vdots & \vdots \\ 1 & \cos\left(\frac{2\pi}{Q}\cdot Q\right) & \sin\left(\frac{2\pi}{Q}\cdot Q\right) & 0 \end{bmatrix} \times \begin{bmatrix} S_0 \\ S_1 \\ S_2 \\ S_3 \end{bmatrix} =$$

$$\tfrac{\mu}{2}\begin{bmatrix} S_0 + S_1\cos\left(\frac{4\pi}{Q}\cdot 0\right) + S_2\sin\left(\frac{4\pi}{Q}\cdot 0\right) \\ S_0 + S_1\cos\left(\frac{4\pi}{Q}\cdot 1\right) + S_2\sin\left(\frac{4\pi}{Q}\cdot 1\right) \\ \vdots \\ S_0 + S_1\cos\left(\frac{4\pi}{Q}\cdot Q\right) + S_2\sin\left(\frac{4\pi}{Q}\cdot Q\right) \end{bmatrix} \tag{7}$$

In the last equation the last column has been removed since without the phase retarder parameter S_3 cannot be obtained from the measurement and $S_3 \equiv 0$ is assumed. Response P_m can be also expressed in terms of Fourier's series as:

$$P_m = a_0 + \textstyle\sum_k a_k \cos(km\theta) + b_k \sin(km\theta), \tag{8}$$

where θ is the analysers angular increment between the measurements. Fourier coefficients can be calculated as:

$$a_0 = \tfrac{1}{Q}\textstyle\sum_{m=0}^{Q-1} P_m\,,\; a_k = \tfrac{2}{Q}\textstyle\sum_{m=0}^{Q-1} P_m \cos\left(\tfrac{2\pi}{Q}km\right),$$

$$b_k = \tfrac{2}{Q}\textstyle\sum_{m=0}^{Q-1} P_m \sin\left(\tfrac{2\pi}{Q}km\right). \tag{9}$$

By comparing Eqs. (8) and (7), it can be found that the Stokes parameters are encoded in Fourier coefficients:

$$\widehat{S_1} = a_1,\; \widehat{S_2} = b_1,\; \widehat{S_0} = a_0, \tag{10}$$

where $\widehat{S_1}$, $\widehat{S_2}$, and $\widehat{S_0}$ denote the estimated parameters of the Stokes vector.

The number of recorded Q states should be at least 2K + 1, where K denotes the number of the highest harmonic that one wants to include in the measurement. Determination of the Stokes parameters via Fourier transformation automatically yields the best-fit solution of measurement data in terms of the sum of the least squares. This method is computationally effective and additionally higher harmonics of the recorded signal can be used to diagnose the polarimeter systematic errors, including beam-wandering [2]. Appropriate analysis of higher harmonics and other spurious frequencies can serve as measurement quality gauge.

3.3 Phase-locked methods

Since the detector is only sensitive to the radiation power, only the S_0 parameter of the Stokes vector is recorded; accordingly, only the first row of the Mueller

matrix of the polarizer is required to analyse the polarization state of radiation. The measured radiance value for a single detector in FPA is:

$$I_m = \frac{\mu}{2}(S_0 + S_1\cos(2\omega t) + S_2\sin(2\omega t)). \quad (11)$$

By multiplying the measured signal by two harmonic reference signals (synphase and quadrature), which are phase-shifted by $\pi/2$ and averaged over time (low-pass filter), one can obtain the information about the Stokes parameters of the incident radiation:

$$S_0 = \frac{2}{\mu Q}\sum_{m=1}^{Q} I_m(t)$$

$$S_1 = \frac{4}{\mu Q}\sum_{m=1}^{Q} I_m(t)\cos(2\omega t) \quad (12)$$

$$S_2 = \frac{4}{\mu Q}\sum_{m=1}^{Q} I_m(t)\sin(2\omega t).$$

This method is applicable to time-division polarimeters.

4. Brief systems comparison

The most complex system is a hyperspectral polarimeter, in which the full Stokes vector can be determined for each recorded wavelength separately. The simplest in terms of construction is a single-band, snapshot polarimeter in which the circular polarization is omitted. Determining the circular polarization requires an additional delay element. Since the contribution of a circularly polarized radiation in the observed scene is small [1], the circular polarization is often neglected, thereby simplifying the device design.

Division of amplitude systems is difficult to align properly due to a large number of alignment degrees of freedom and strict requirements on the image alignment. According to different authors, images should be aligned at least within ¼ of a pixel, some authors suggesting even 1/10 of a pixel [34] what is considered to be virtually impossible to achieve for this kind of system [4,24,27]. Moreover, this alignment is difficult to maintain long-term especially in a wide range of ambient temperatures. The cost of building these systems is high as multiple matrices are required for imaging each Stokes parameter on a separate detector.

Division of aperture systems are easier to align and usually will have a better long-term stability compared to division of amplitude systems. Since all the polarization states are mapped onto one FPA, the spatial resolution is degraded. This system requires a field stop to sharply separate individual channels on the array. However, in the case of uncooled LWIR systems, the field stop would act as a strong source of radiation, resulting in an additional spurious signal.

Division of focal plane polarimeters require micropolarier arrays or specialized FPA detectors that are sensitive to the defined polarization state. The FPA technology of micropolarizers requires dedicated technological processes for the elements production. Polarimeters of this type are, by definition, subject to a registration error, which is removed at the stage of final signal processing; however, their optical design is significantly simpler compared to the previously discussed solutions. The basic pros and cons of the design solutions for various imaging polarimeters are summarized in Table 1. Furthermore, Tables 2 and 3 present polarimetric-image-processing combability matrix and polarimetric-image-processing comparison, respectively.

Table 1
Comparison of image-polarimeter architectures.

Architecture	Advantages	Disadvantages
Division of amplitude	simultaneous registration of all polarization states	- complicated mechanical adjustment - IFOV error - high cost
Division of time	simplest built straightforward data analysis	- beam-wandering - dynamic scene registration error - offline or high-latency processing
Division of aperture	simultaneous registration of all polarization states	- loss of spatial resolution - complicated optical train
Division of FPA	simultaneous registration of all polarization states	- low component availability - IFOV error
Spectropolarimeters	circular polarization is easily achievable	- low frame rate - high complexity

Table 2
Polarimetric-image-processing combability matrix.

Architecture	Data-reduction matrix	Frequency analysis	Phase-locked methods
Division of amplitude	×		
Division of time	×	×	×
Division of aperture	×		
Division of FPA	×		
Spectropolarimeters	×	×	×

Table 3
Polarimetric-image-processing comparison.

Processing method	Advantages	Disadvantages
Data-reduction matrix	- direct application of the Stokes theory - straightforward physical interpretation	- demand for a consistent optical signal
Frequency analysis	- spectral noise shaping - additional measurement quality gauges	- constant sampling rate - limited applications
Phase-locked methods	- noise-filtering	- requires a phase-synchronization loop - limited applications

Considering economic reasons and construction simplicity, the most advantageous solution is the time-division one. To register dynamic objects, the rotation period of the polarizing element should be as small as possible. However, in this type of solution, the biggest disadvantages are as follows: reduction in the frequency of obtained results, need to register relatively static objects, and a significant number of picture frames required to determine the result, thereby resulting in high-latency computations.

5. Future perspectives

Imaging polarimetry is a powerful tool for enhancing the information available in various remote sensing applications. For a remote object detection, LWIR polarimetric imagers have been driven by particular applications, especially military applications, which include remote sensing cameras developed to detect masked objects such as Improvised Explosive Devices and drones. Non-military applications emerged especially in domains such as environmental monitoring (e.g., oil spills), biological-tissue examination, and biometry for face recognition. Compact polarimeters can be used in airborne applications on small unmanned aircrafts, making them available for civilian applications such as crop monitoring, and firefighting-squad aid on search and rescue missions. Additional information regarding the orientation of surfaces of objects and dominant energy source can be used to extract additional information about the object geometry making it possible to estimate the three-dimensional structures of objects located at far off distances. This can be especially helpful in the detection and identification in security applications, providing additional information about the object geometry, thereby presenting better identification probabilities. Additionally, the recent advances in deep-learning methods can help utilize additional information even more.

6. Conclusions

A brief survey of polarimetric systems is presented, with focus on architectures and data processing in the Stokes polarimeters used in a remote object detection. The state-of-the-art polarimeters and predictions were also discussed. Because of the rapid progress in the infrared-detector technology, highly sensitive polarimetric imagers operating especially in the 8–12 μm spectral band might emerge in the near future. Such devices might generate significant interest, especially for a wide range of potential applications outlined in the Introduction and Section 5. Therefore, the future of imaging polarimetry appears promising.

References

[1] Tyo, S. J., Goldstein, D. L., Chenault, D. B. & Shaw, J. A. Review of passive imaging polarimetry for remote sensing applications. *Appl. Opt.* **45**, 5453–5469 (2006). https://doi.org/10.1364/AO.45.005453

[2] Kudenov, M. W., Pezzaniti, J. L. & Gerhart, G. R. Microbolometer-infrared imaging Stokes polarimeter. *Opt. Eng*. 48, 063201 (2009). https://doi.org/10.1117/1.3156844

[3] Harchanko, J. S., Pezzaniti, L., Chenault, D. & Eades, G. Comparing a MWIR and LWIR polarimetric imager for surface swimmer detection. *Proc. SPIE* **6945**, 69450X (2008). https://doi.org/10.1117/12.778061

[4] Kudenov, M. W., Dereniak, E. L., Pezzaniti, L. & Gerhart, G. R. 2-Cam LWIR imaging Stokes polarimeter. *Proc. SPIE* **6972**, 69720K (2008). https://doi.org/10.1117/12.784796

[5] Rodenhuis, M., Canovas, H., Jeffers, S. V. & Keller, C. U. The Extreme Polarimeter (ExPo): design of a sensitive imaging polarimeter. *Proc. SPIE* **7014**, 70146T (2008). https://doi.org/10.1117/12.788439

[6] van Holstein, R. *et al*. Combining angular differential imaging and accurate polarimetry with SPHERE/IRDIS to characterize young giant exoplanets. *Proc. SPIE* **10400**, 1040015 (2017). https://doi.org/10.1117/12.2272554

[7] Rotbøll, J., Søbjærg, S. & Skou, N. A novel L-Band polarimetric radiometer featuring subharmonic sampling. *Radio Sci.* **38**, 1–7 (2003). https://doi.org/10.1029/2002RS002666

[8] Yueh, S. H. Modeling of wind direction signals in polarimetric sea surface brightness temperatures. *IEEE Trans. Geosci. Remote Sensing* **35**, 1400–1418 (1997). https://doi.org/10.1109/36.649793

[9] Laymon, C. *et al*. MAPIR: An airborne polarimetric imaging radiometer in support of hydrologic satellite observations. in *IEEE Geoscience and Remote Sensing Symposium* 26–30 (2010).

[10] Coulson, K. L., Gray, E. L. & Bouricius, G. M. A study of the reflection and polarization characteristics of selected natural and artificial surfaces. *Tech. Informat. Series* Rep. R64SD74. (General Electric Co., Missile and Space Div., Space Sciences Lab., 1964)

[11] Lafrance, B. & Herman, M. Correction of the Stratospheric Aerosol Radiative Influence in the POLDER Measurements. *IEEE Trans. Geosci. Remote Sensing* **36**, 1599–1608 (1998). https://doi.org/10.1109/36.718863

[12] Hooper, B. A., Baxter, B., Piotrowski, C., Williams, J. Z. & Dugan, J. An airborne imaging multispectral polarimeter (AROSS-MSP). in *Oceans 2009*, 1-10 (2009). https://doi.org/10.23919/OCEANS.2009.5422152

[13] Giakos, G. C. *et al*. Near infrared light interaction with lung cancer cells. in *2011 IEEE International Instrumentation and Measurement Technology Conference* 1–6 (2011). https://doi.org/10.1109/IMTC.2011.5944333

[14] Sobczak, M., Kurzynowski, P., Woźniak, W., Owczarek, M. & Drobczyński, S. Polarimeter for measuring the properties of birefringent media in reflective mode. *Opt. Express* **28**, 249–257 (2020). https://doi.org/10.1364/OE.380998

[15] Sadjadi, F. Electro-Optical Systems for Image Recognition. *LEOS 2001. 14th Annual Meeting of the IEEE Lasers and Electro-Optics Society (Cat. No.01CH37242)* vol. 2 550–551 (2001). https://doi.org/10.1109/LEOS.2001.968933

[16] Bieszczad, G., Gogler, S. & Krupiński, M. Polarization state imaging in long-wave infrared for object detection. *Proc. SPIE* **8897**, 88970R (2013). https://doi.org/10.1117/12.2028858

[17] Gurton, K. P. & Felton, M. Remote detection of buried land-mines and IEDs using LWIR polarimetric imaging. *Opt. Express* **20**, 22344–22359 (2012). https://doi.org/10.1364/OE.20.022344

[18] Więcek, B. & De Mey, G. *Termowizja w podczerwieni. Podstawy i zastosowania*. (Warszawa: Wydawnictwo Pomiary Automatyka Kontrola, 2011). [in Polish]

[19] Rogalski, A. *Infrared detectors*. (Amsterdam: Gordon and Breach Science Publishers, 2000).

[20] Chenault, D., Foster, J., Pezzaniti, L., Harchanko, J. & Aycock, T. Polarimetric sensor systems for airborne ISR. *Proc. SPIE* **9076**, 90760K (2014). https://doi.org/10.1117/12.2053918

[21] Holtsberry, B. L. & Voelz, D. G. Material identification from remote sensing of polarized self-emission. *Proc. SPIE* **11132**, 1113203 (2019). https://doi.org/10.1117/12.2528282

[22] Madura, H., *Pomiary termowizyjne w praktyce : praca zbiorowa*. (Agenda Wydawnicza PAKu, 2004). [in Polish]

[23] Baas, M., *Handbook of Optics*. (New York: McGraw-Hill, 1995).

[24] Eriksson, J., Bergström, D. & Renhorn, I. Characterization and performance of an LWIR polarimetric imager. *Proc. SPIE* **10434**, 1043407 (2017). https://doi.org/10.1117/12.2278502

[25] Gogler, S., Bieszczad, G. & Swiderski, J. Method of signal processing in a time-division LWIR image polarimetric sensor.

Appl. Opt. **59**, 7268–7278 (2020). https://doi.org/10.1364/AO.396675

[26] Cremer, F., de Jongm, W. & Schutte, K. Infrared polarization measurements and modeling applied to surface-laid antipersonnel landmines. *Opt. Eng*. **41**, 1021–1032 (2002). https://doi.org/10.1117/1.1467362

[27] Pezzaniti, L. J. & Chenault, D. B. A divison of aperture MWIR imaging polarimeter. *Proc. SPIE* **5888**, 58880 (2005). https://doi.org/10.1117/12.623543

[28] Chun, C. S. L., Fleming, D. L., Harvey, W. A. & Torok, E. J. Target discrimination using a polarization sensitive thermal imaging sensor. *Proc. SPIE* **3062**, 60–67 (1997). https://doi.org/10.1117/12.327165

[29] Moxtek. https://moxtek.com/ (2020).

[30] Stokes, R. J., Normand, E. L., Carrie, I. D., Foulger, B. & Lewis, C. Develepment of a QCL based IR polarimetric system for the stand-off detection and location of IEDs. *Proc. SPIE* **7486**, 748609 (2009). https://doi.org/10.1117/12.830076

[31] Chenault D. B., Vaden, J. P., Mitchell, D. A. & Demicco, E. D. New IR polarimeter for improved detection of oil on water. *SPIE Newsroom* (2017). https://doi.org/10.1117/2.1201610.006717

[32] Tyo, S. J. & Turner, T. S. Variable-retardance, Fourier-transform imaging spectropolarimeters for visible spectrum remote sensing. *Appl. Opt*. **40**, 1450–1458 (2001). https://doi.org/10.1364/AO.40.001450

[33] Craven-Jones, J., Way, B. M., Hunt, J., Kudenov, M. W. & Mercier, J. A. Thermally stable imaging channeled spectropolarimetry. *Proc. SPIE* **8873**, 88730J (2013). https://doi.org/10.1117/12.2024112

[34] Smith, M. H., Woodruff, J. B. & Howe, J. D. Beam wander considerations in imaging polarimetry. *Proc. SPIE* **3754**, 50–54 (1999). https://doi.org/10.1117/12.366359